Thermochromic Nanocrystalline Au-VO_2 Composite Thin Films Prepared by Radiofrequency Inverted Cylindrical Magnetron Sputtering

J.B. Kana Kana[a, b,c,d*], J.M. Ndjaka[c,d], B.D. Ngom[a,c], N. Manyala[c,e], O. Nemraoui[f], A.Y. Fasasi[c,g], R. Nemutudi[a], A. Gibaud[h], D. Knoesen[b], M. Maaza[a,c]

[a] Nanoscience and Nanotechnology laboratories, Materials Research Department, iThemba LABS, P.O. Box 722, Somerset West 7129, South Africa

[b] Department of Physics, University of the Western Cape, Private Bag X17, Bellville 7535, South Africa

[c] African Laser Centre, P.O. Box 395, Pretoria 0001, South Africa

[d] Department of Physics, University of Yaounde I, P.O. Box 812, Yaounde, Cameroon

[e] Institute of Applied Materials, University of Pretoria, Pretoria 0002, South Africa

[f] Department of Physics and Engineering, University of Zululand, Private Bag X1001, Kwadlangezwa 3886, South Africa

[g] Centre for Energy Research & Development, Obafemi Awolowo University, Ile-Ife, Osun State, Nigeria

[h] Laboratoire de Physique de L'Etat Condensé, Université du Maine, Le Mans, France

Corresponding author: J.B. Kana Kana

Postal address: Nanoscience and Nanotechnology laboratories, Materials Research Dept, iThemba LABS, P.O. Box 722, Somerset West 7129, South Africa

Email address: jbkana@tlabs.ac.za, jbkana@gmail.com

Tel: +27218431145/6, Fax: +27218433543

Abstract

Highly crystalline Au-VO_2 nanocomposite thin films were prepared on Corning glass substrates by reactive radiofrequency inverted cylindrical magnetron sputtering (ICMS). It is a low cost potential coating technology for the production of large area uniform nanocomposite thin films exhibiting plasmonic properties. This paper reports the synthesis and feasibility of reliably reproduced high quality of Au-VO_2 by ICMS. Structural, morphological, interfacial analysis and optical properties of synthesized Au-VO_2 nanocomposite thin films are reported.

PACS: 81.07.-b; 68.55.jk; 78.67.-n

Keywords: Inverted cylindrical magnetron sputtering; Thin films; Nanocomposite; Surface plasmon resonance; Plasmonic materials

1. Introduction

Nanocomposite consisting of noble metal nanoparticles (Au, Ag or Cu) embedded in a dielectric matrix attracted much attention recently because of their large number of potential applications, which include ultrafast optical switches due to their nonlinear susceptibilities and fast response time [1, 2], surface enhanced spectroscopies, biomedical sensors [3-5], thermally optical switches or coatings [6], optical sensing [5,7], photothermal medical therapeutics and solar glazing [8]. The wavelength tuning of the surface plasmon resonance is highly desirable in the applications of the metallic nanoparticles. Since the surface plasmon resonance wavelength (λ_{SPR}) depends on their particle size, shape, inter-

particle distance and the dielectric function of the surrounding host [9-13], the tunable λ_{SPR} in the visible and near infrared regions has been achieved by changing these parameters of the metallic nanoparticles [9-14]. Recently, a great interest has been made to tune λ_{SPR} of noble metal nanoparticles by using dielectric functional materials such as thermochromic [15-18], electrochromic [19] or photochromic [20], as the matrices. The use of dielectric functional materials as the matrices opens a range of possibilities for tuning the λ_{SPR} in a controllable manner. Recently, the effect of external temperature stimuli on the plasmon resonance of Au or Ag nanoparticles embedded in a thermochromic VO_2 matrix, of composite Au-VO_2 [17,18] or Au-on-VO_2 core shell particles [8,21] or Ag on top of VO_2 [15] has been sparsely explored with only few reports. It is well-known that VO_2 undergoes a reversible first-order phase transition from semiconductor to metal at critical temperature Tc = 68 ^{o}C, accompanied by large change in optical properties in the infrared region [22-24] which will be exploited to modulate the λ_{SPR}.

So far we are aware of few reports to date on nanocomposite films consisting of noble metal nanoparticles of Au or Ag embedded in a thermochromic VO_2 matrix by some researchers. Maaza et al. synthesized Au-VO_2 films by off-axis pulsed laser deposition and presented a method to thermally tune the surface plasmon frequency in a controllable manner [17, 18]. Xu et al. sputtered silver (Ag) and gold (Au) on top of a VO_2 thin film by planar radiofrequency (rf) magnetron sputtering, showed the dependence of the silver nanoparticles localized surface plasmon resonance (LSPR) wavelength position on the silver mass thickness [15] and demonstrated that Au nanoparticles have a marked effect on the reduction in the phase transition temperature of VO_2 [25] respectively. The modulation of the LSPR on lithographically fabricated gold nanoparticles arrays on VO_2 overlayer

deposited by pulsed laser deposition was reported by Suh et al. [16]. Aggregates of gold spheres in a matrix of VO_2 prepared by Sol-gel method was investigated by Cavanna et al. in order to carry out the optical switching performances of this nanocomposite [26]. The synthesis of gold doped vanadium dioxide by hybrid aerosol assisted and atmospheric pressure chemical vapor deposition was recently presented by Binions et al. [27].

The reactive sputtering process is a widely used coating technique for the production of oxides, nitrides, carbides and nanocomposites. The main drawbacks of this process are the hysteresis behavior, which seriously limit the stability, the poisoning of the sputtering target, which substantially reduces the sputter erosion rate, the stability control and arcing effect. Considerable efforts have been devoted to eliminate these drawbacks such as (i) increasing the pumping speed, which requires larger additional costs; (ii) increasing the target-to-substrate distance, which requires larger chambers (hence, higher costs); (iii) plasma emission monitoring; (iv) pulsed reactive gas flow, which requires an amount of optimization and a continuous monitoring and adjustment of the process; (v) dual magnetrons or magnetron with a full target erosion; (vi) substoichiometric ceramic target; (vii) voltage control [28, 29]. Planar reactive magnetron sputtering suffers most of these undesirable phenomena. Planar sputtering also suffers from being a line-of-sight process and is not well suited for coating non-planar substrates. Inverted cylindrical magnetron sputtering (ICMS) also known as hollow cathode sputtering is used to sputter from the inner surface of cylindrical targets and produce highly conformal coatings [30]. Due to its enclosed geometry, it also produces intense and very uniform plasma next to the target surface that results in high deposition rates [31]. Hollow cathodes also lead to excellent target erosion because the sputtered atoms that are not deposited on the substrate

get redeposited on the cathode. An additional advantage of hollow cathodes is their lower target cost and they produce large area uniform films [32, 33]. Despite the main feature of pulsed laser deposition (PLD) which is that the stoichiometry of the target can be retained in the deposited films, the major problems of PLD are splashing or microparticulates deposition on the films which greatly affect the growth and the properties of the films and the narrow angular distribution of the ablated species. These drawbacks limit the usefulness of PLD in producing large area uniform thin films. Production related issues of PLD concerning reproducibility [34], large-area scale-up [35] have begun to be addressed. Recently, some technological issues have been addressed on the hollow cathode sputtering. Lindberg et al. [36] reported the hysteresis behavior in the target voltage while depositing Al-O films. They used a hollow cathode magnetron with a low- frequency AC power. Such setup resembles a dual target magnetron sputtering rather than a hollow cathode source. Pradhan et al. [37] reported that, the hollow cathode does not exhibit the hysteresis behavior generally observed in planar reactive sputtering systems and is stable at all operating points without any feedback control. They explained the absence of the hysteresis behavior on the basis of the enclosed geometry, which significantly reduces the sputtered flux leaving the hollow cathode sputtering. These properties strongly indicate that hollow cathode sputtering has sufficient possibilities to prepare “smart” class of nanocomposite films with a wide range of technological applications. A possibility to form nanocomposite thin films of Au-VO_2 by reactive ICMS is demonstrated.

This article reports on the preparation of highly nanocrystalline Au-VO_2 composite thin films by rf-inverted cylindrical magnetron sputtering. The structural, morphological and optical properties of the synthesized films have been studied. Our results have been

compared to those previously reported for Au-VO_2 films prepared by other deposition techniques.

2. Experimental details

2.1. Sample preparation

A cylindrical vanadium metal sheet 99.98 % purity (Alfa Aesar) 5 cm in diameter and 2.5 cm long with a triangular slice of high purity gold 99.99 % (metal basis) 1 mm thick carefully stuck by silver paint on the wall of the cylindrical vanadium metal, was used as a target. This target was mounted on the cathode of the sputter gun, also called an Inverted Cylindrical magnetron (ICM) gun or hollow cathode source. The ICM gun is mounted in a double cross-piece vacuum chamber on a standard DN 100 CF flange with a mounting depth of 12 cm. The Corning glass substrates (glass number 0810401) were ultrasonically cleaned in acetone and subsequently in ethanol for 10 min, respectively, rinsed in des-ionized water and then dried in the oven at 100 ^{o}C. The dried substrates were glued with silver paint onto the heated substrates holder perpendicular to the target and along its central axis as illustrated in Figure 1. The position of the substrate was a crucial parameter to fabricate high quality of films exhibiting plasmonic features. The substrates placed at any position inside the hollow cathode revealed a pure gold metallic character in few minutes of deposition because of the fast sputtering of gold slice stuck on the wall of the cylindrical vanadium metal. Films exhibiting pure gold metallic character do not show any plasmon resonance feature as reported by Xenogiannopoulou et al. [38]. The distance of 2 cm from substrate holder to sputtering head of our configuration adopted and shown in Figure 1 was an optimal distance to fabricate good quality of films revealing plasmonic feature. This position only leads to low deposition rate because the plasma is just collected at the exit of

the hollow cathode. Other positions further than 2 cm lead to even lower deposition rate. The temperature of the sample holder was controlled using a k-type thermocouple connected to a 3216 PID controller supplied by Eurotherm. After pumping the deposition chamber to a base pressure of 5 x 10^{-4} Pa, the chamber was backfilled with a mixture of 10 % O_2 in Ar followed by high-purity Ar. The discharge was ignited in a mixture of O_2/Ar (4.44 % O_2 concentration) with a total working pressure of 1.8 Pa. This pressure is higher than what is typically used for planar magnetron sputtering. Such high pressure is needed for a smooth operation of the hollow cathode sputtering. A very high total pressure of 8.67 Pa was obtained by Pradhan et al. [37] using hollow cathode sputtering to deposit alumina thin films. The low oxygen concentration of 4.44 % was sufficient to completely poison the target. Hence, it was well demonstrated by Pradhan et al. [37] that the transition from metallic to poison mode with hollow cathode sputtering occurs gradually at very low oxygen concentrations while in planar sputtering this transition occurs abruptly at higher oxygen concentrations. In the same trend, Delahoy and co-workers [39] reported that only a very small amount of oxygen is sufficient to immediately oxidize (poison) the target if the oxygen passes through the cathode of hollow cathode sputtering. We believe that this is due to the enclosed geometry of the hollow cathode sputtering, which confines most of the sputtered atoms and ions within the hollow cathode. The ICM gun was operated at a power of 70 W using a Dressler Cesar (13.56 MHz) rf power generator for 45 min. Copper cooling water tubes wrapped around the circumference of the hollow cathode were used to cool the ICM gun during operation. A pre-sputtering time of 30 min was used to remove surface contamination and oxides on the target and to ensure stabilized sputtering conditions. In this work, Au-VO_2 nanocomposites films were prepared at different substrate temperatures

ranging from 400 ^{o}C to 600 ^{o}C. The thickness of the sputtered Au-VO_2 films ranges from 64 to 70 nm .The volume fraction of gold in the sputtered samples was found to be slightly changed and ranges from 6.3 to 6.9 % as determined by simulation of experimental X-ray reflectivity profiles.

2.2. Sample evaluation

The crystalline structure of the Au-VO_2 composite thin films was determined by X-ray diffractometry (XRD) in a θ-2θ mode with CuKα (AXS Bruker).The surface morphology of the films was observed by atomic force microscopy (AFM) using Nanoscope III a, Digital Instruments operated in tapping mode under ambient conditions. X-ray reflectivity at wavelength of 1.54 Å on a Panalytical X-pert reflectometer of the "Laboratoire de Physique de l'Etat Condensé-Université du Maine." was used for the analysis of surface and interface of the films. The plasmonic properties and thermochromic behavior of the synthesized films were examined by using a Spectrophotometer (CECIL 2000) incorporated with Peltier thermoelectric heating and cooling stage.

3. Results and discussion

3.1. Film structure

Figure 2 shows the XRD patterns of Au-VO_2 nanocomposite films sputtered in the substrate temperature range of 400-600 ^{o}C. These films were deposited on Corning glass substrates. There are diffraction peaks for both Au and VO_2 in the synthesized films. This indicates that both components were crystallized. The spectra exhibited seven peaks in the 2θ range 20-70 ^{o}, four of which correspond to the VO_2 monoclinic (011), (002), (220) and

(022) planes, and the other three peaks (111), (200), (220) are assigned to gold fcc. The same peaks occur in all the spectra for different temperatures, but their relative intensity changes. The VO_2 (002) peak gradually disappears with increasing substrate temperature and completely disappears at substrate temperature of 600 ^oC. Also, the VO_2 (220) and (022) peaks show a relative variation of intensity. This indicates that a texture of the host matrix VO_2 may change with increasing substrate temperature. The intensity in all gold peaks increases with increasing deposition temperature and we noticed that the higher the substrate temperature, the sharper are the gold peaks. From the strongest Au (111) and VO_2 (011) peak width, the size of the gold and VO_2 particle was calculated using Scherrer's formula [40]. Figure 3 shows the relationship between the Au and VO_2 particle size and the substrate temperature. It can be seen that the Au and VO_2 particle size both increased upon increasing substrate temperature. The Au particles first grew rapidly from 9.9 nm to 25.4 nm in the substrate temperature range of 400-500 ^oC, but then slightly decreased or saturated for substrate temperature higher than 500 ^oC. The VO_2 particle size increased linearly with increasing substrate temperature in the range of 400-550 ^oC and then dropped slightly at substrate temperature of 600 ^oC.

3.2. Film surface morphology

AFM images of Au-VO_2 nanocomposite films were taken to determine dependence of surface morphology on substrate temperature. Figure 4 (a) and (b) show AFM images of samples sputtered at substrate temperature (Ts) of 400 ^oC and 600 ^oC, respectively. From the two-dimensional (2D) images it can be seen that the surface morphologies vary significantly among the films grown at different substrate temperature. It seems that the

Au-VO_2 films sputtered at 400 ^oC as shown in Figure 4 (a), is composed of small conical-like islands dispersed with a low height of 6.14 nm, whereas those sputtered at higher substrate temperature of 600 ^oC as Figure 4 (b) consist of very compact large conical-like islands with a significant height of 19.25 nm. The root mean square roughness shows 1.88 and 5.81 nm for Ts = 400 and 600 ^oC, respectively.

3.3. Surface and interface analysis

Figure 5 shows the typical X-ray reflectivity profile of Au-VO_2 films sputtered at 550 ^oC. It is clearly shown that, at small grazing angles, the incoming beam is totally reflected giving rise to the plateau of total reflection, over this region, usual interference fringes so called "Kiessig fringes" due to the finite film thickness are observed. The simulation of total reflection plateau and Kiessig fringes allow to deduce the mean electron density, total thickness, roughness at film surface and interfacial roughness. The extracted parameters from the electron density profile shown in inset of Figure 4 are: σ_o = 3.8 nm, σ_1 = 2.4 nm and MED = 1.5 $Å^{-3}$, where σ_o, σ_1 represent roughness at film surface and film/substrate interface, respectively, and MED the mean electron density. To obtain a better fit, an interfacial layer of 1.8 nm thickness was taken into account. The surface roughness of Au-VO_2 composite thin film sputtered at 550 ^oC was compared by both methods XRR and AFM. AFM image of this film (not shown here) very similar to the one sputtered at 600 ^oC , revealed a compact large conical-like islands on the surface with significant height of 19.30 nm and a root mean square roughness (σ_{AFM}) of 5.94 nm. By comparing the roughness at film surface obtained by XRR (σ_o = 3.8 nm) and AFM (σ_{AFM} = 5.94 nm), a huge difference is clearly observed. This can be explained by the fact that, the results of XRR and AFM measurements essentially depend on the irregularity of a surface and on the

type of roughness. It is known that for very flat surfaces (with a root mean square roughness in the range of several angstroms) XRR and AFM give coincident roughness parameters [41, 42]. When the surface has high irregularities such as knobs, islands with a complicated height distribution a significant discrepancy between roughness parameters obtained by both methods is observed [43, 44]. Generally the surfaces having such irregularities are mostly non-gaussian surfaces. The discrepancy between estimations of roughness parameters derived by both techniques for non-gaussian surfaces is reported by Mironov et al. [45].

3.4 Plasmonic properties

3.4.1. *Surface plasmon resonance wavelength shift and thermochromic behavior*

The optical transmittance spectra of the Au-VO_2 samples sputtered at different substrate temperatures are shown in Figure 6. The spectral transmittance of the resulting films at low-temperature semiconducting phase and high-temperature metal phase are sharply contrasting in the near-infrared region due to the thermochromism properties of the host matrix VO_2. It can be noticed that, at higher substrate temperature, the thermal switching of the semiconductor-metal transition is less pronounced. The peak absorption of small gold nanoparticles observed in the minimum of the spectral transmittance is clearly appeared in the visible region range of 590-670 nm for all sputtered samples. This peak absorption corresponds to the gold peak surface plasmon resonance (SPR). This resonant electromagnetic behavior of noble-metal nanoparticles is due to the confinement of the conduction electrons to the small particle volume. It is interesting to find that the surface plasmon resonance wavelength (λ_{SPR}) for all the samples blue shifts when the external temperature increases from 20 ^{o}C to 100 ^{o}C (heating process).Due to the reversibility of

the phase transition of the host matrix, λ_{SPR} red shifts when the external temperature decreases from 100 ^{o}C to 20 ^{o}C (cooling process).

The influence of substrate temperature, T_S, on λ_{SPR} seems to be significant. Increase in Ts not only leads to a red shift of λ_{SPR} for both phases (semiconductor and metal) when the external temperature is below and above the transition temperature $T_{C,}$ but also enhances the difference in λ_{SPR}, namely $\Delta\lambda_{SPR}$, between the two phases of VO_2. For sample sputtered at Ts = 400 ^{o}C, the λ_{SPR} position is 635 nm below Tc, and 599 nm above Tc, with a difference $\Delta\lambda_{SPR}$ = 36 nm. In contrast, for sample sputtered at Ts = 450 ^{o}C, λ_{SPR} locates at 657 nm below Tc, and at 610 nm above Tc, with $\Delta\lambda_{SPR}$ = 47 nm. However, for samples sputtered at 500, 550 and 600 ^{o}C the λ_{SPR} position was the same 665 nm below Tc, and 608 nm above Tc, with a difference $\Delta\lambda_{SPR}$ = 57 nm. This clearly indicates that the λ_{SPR} shift to red as Ts increases. This red shift of λ_{SPR} with Ts increasing is consistent with an increase in the particle size of the Au nanoparticles revealed by XRD in the nanocomposite films; i.e., larger Au nanoparticles exhibit red-shifted SPR absorption [5, 46]. A significant enhancement of $\Delta\lambda_{SPR}$ with increasing T_S results from the significant difference in dielectric constant of the host matrix VO_2. In comparison to λ_{SPR} shift observed from Au-VO_2 nanocomposites synthesized by pulsed laser ablation [18] or gold-doped VO_2 produced by hybrid aerosol assisted and atmospheric pressure chemical vapor deposition [27], there is a comparable shift of λ_{SPR} of 45 nm obtained from the sample sputtered at 450 ^{o}C and an enhanced shift of λ_{SPR} of 57 nm obtained from the sample sputtered at 600 ^{o}C.

In order to compare the phase transition characteristics of Au-VO_2 and pure VO_2 films, the transmittance at wavelength of 1100 nm at different external temperature stimuli was taken. All of the films show thermochromic behavior with transition temperature and

width of hysteresis dependent on the substrate temperature. Figure 7 shows the hysteresis behavior at 1100 nm of samples sputtered at 400 and 600 ^{o}C. The transition temperature is defined as the minimum of the derivative curve of the heating curve of the hysteresis loop. The hysteresis width was evaluated as the difference between the transition temperature of heating and cooling curve of the hysteresis loop. The sharpness and hysteresis width of 10 ^{o}C of Au-VO_2 thin films sputtered at 400 ^{o}C are comparable to those observed of pure polycrystalline VO_2 sputtered by ICMS at the same substrate temperature [24]. A wide hysteresis width of 20 ^{o}C obtained for Au-VO_2 film sputtered at 600 ^{o}C is probably due to the thermal stress. By comparison, samples of Au-VO_2 sputtered at substrate temperature range 400-500 ^{o}C produced by ICMS showed a transition temperature of 60-70 ^{o}C and an optical hysteresis width of 10-15 ^{o}C similar to those produced by classical sputtering or Sol-gel [25, 26]. Those sputtered at high substrate temperatures 550-600 ^{o}C gave hysteresis width of 20 ^{o}C similar to gold-doped VO_2 films prepared by hybrid aerosol assisted-CVD [27]. A high transition temperature of 80 ^{o}C was obtained for Au-VO_2 sputtered at high substrate temperatures. A similar shift of transition temperature towards a higher temperature has been reported by Futaki et al. [47] for Ti or Ge doped VO_2.

3.4.2. *Surface plasmon resonance hysteresis*

Figure 8 displays the absorbance versus wavelength of Au-VO_2 films sputtered at substrate temperature of 400 ^{o}C and 600 ^{o}C. The strength of the plasmon resonance peak of gold is clearly observed as well as the shift of plasmon resonance aforementioned. In order to study the external temperature dependence of λ_{SPR}, the absorbance measurements were taken during the rise and drop of external temperature. The wavelength at absorbance maximum corresponds to λ_{SPR}. Figure 9 displays the temperature-dependent hysteresis of

the λ_{SPR}. The SPR hysteresis behavior is similar to the optical hysteresis shown in Figure 7. It can be seen that the Au-VO_2 sputtered at 400 ^oC revealed a hysteresis width of 10 ^oC with an abrupt variation of λ_{SPR} at 65 ^oC. The sharpness of the variation of the λ_{SPR} in the vicinity of the transition temperature of single crystal VO_2 confirms the high quality of the host matrix VO_2. In comparison to SPR hysteresis observed from Au-VO_2 nanocomposites produced by laser ablation [18], the hysteresis width, abrupt variation of λ_{SPR} at 65 ^oC and sharpness are almost the same. The sample sputtered at high substrate temperature of 600 ^oC revealed a wide SPR hysteresis width of 20 ^oC and it indicates an abrupt fall of λ_{SPR} around 85 ^oC. In comparison to SPR hysteresis observed from Au-VO_2 sputtered at 600 ^oC produced by hybrid aerosol assisted-chemical vapor deposition [27], the hysteresis width of 20 ^oC is similar and comparable. These anomalous SPR hysteresis characteristics of Au-VO_2 films sputtered at higher substrate temperatures could be due to the thermal stress or microstructures of the synthesized films. Since, it is commonly assumed in the VO_2 thin-film literature that, given a controlled oxide stoichiometry, the sharpness of the phase transition [48] as well as its hysteresis width and critical temperature are dependent on the stress [49] and microstructure of the films [50].

4. Conclusion

"Smart" thermochromic nanocomposite thin films consisting of gold nanoparticles embedded in a thermochromic VO_2 matrix were prepared by ICMS. The structural, morphological, and plasmonic properties of Au-VO_2 synthesized films have been studied. The plasmonic properties and thermochromic behavior of the synthesized nanocomposites films of Au-VO_2 by ICMS are comparable to those seen previously with Au-VO_2 thin films grown by laser ablation, classical sputtering or other conventional coating techniques. This

coating technology offers advantages over others physical vapor deposition such as laser ablation, planar reactive magnetron sputtering. It promises to be fully reproducible and suitable for the synthesis of Au-VO_2 composites thin films.

Acknowledgments

The financial support from the African Laser Centre and Nanosciences African Network is gratefully acknowledged. iThemba LABS-National Research Foundation of South Africa is also acknowledged for support including research equipment and materials. The continuous technical support of Karl Springhorn and Jan Crafford is highly appreciated. Special thanks are due to the reviewer for his fruitful comments.

References

[1] I. Tanahashi, H. Inouye, A. Mito, Jpn. J. Appl. Phys. 42 (2003) 3467.

[2] H. Liao, W. Wen, G.K.L. Wong and G.Yang, 28 (2003) 1790.

[3] K.A.Willets, R.P.Van Duyne, Annu. Rev. Phys. Chem. 58 (2007)267.

[4] C.L.Haynes and R.P.Van Duyne, Nanosphere, J. Phys. Chem. B 105 (2001) 5599.

[5] S.A. Maier, Plasmonics: Fundamentals and Applications, Springer, 2007, p. 74,177.

[6] M.B.Cortie, A.Maaroof and G. Smith, Symposium R: Meta-Materials at the Milli-, Micro-, and Nanoscale, Materials Research Society Fall Conference, Boston, USA, November 28-30, 2006, paper R6.4.

[7] S.Enoch, R.Quidant, G.Badenes, Opt. Express. 12 (2004) 3422.

[8] M.B. Cortie, A. Dowd, N. Harris, and M.J. Ford, Phys. Rev. B 75 (2007)113405.

[9] R.Gupta, M.J.Dyer, and W.A.Weimer, J. Appl. Phys. 92 (2002) 5264

[10] T.R.Jensen, M.D.Malinsky, C.L.Haynes, and R.P.Van Duyne, J.Phys. Chem.B.104 (2000) 10549**.**

[11] G. Xu, M. Tazawa, P.Jin, S. Nakao, and K. Yoshimura, Appl. Phys. Lett. 82 (2003) 3811.

[12] U. Kreibig and M. Vollmer, Optical Properties of Metal Clusters, Springer, Berlin, 1995, p.532.

[13] S.A.Maier and H.A.Atwater, J. Appl. Phys. 98 (2005) 011101.

[14] M.Hirai, A.Kumar, J. Appl. Phys. 100 (2006) 014309.

[15] G.Xu, Y.Chen, M.Tazawa, P. Jin, J. Phys. Chem. B 110 (2006) 2051.

[16] J.Y. Suh, E.U. Donev, D.W. Ferrara, K.A. Tetz, L.C. Feldman and R.F. Haglund Jr., J. Opt. A: Pure Appl. Opt. 10 (2008) 055202.

[17] M. Maaza, O. Nemraoui, C. Sella, A.C. Beye, Gold Bull. 38 (2005) 100.

[18] M. Maaza, O. Nemraoui, C. Sella, A.C. Beye, B. Baruch-Barack, Opt. Commun. 254 (2005) 188.

[19] Z.Wang, G.Chumanov, Adv. Mater. 15 (2003) 1285.

[20] Y.Ohko, T.Tatsuma, T.Fujii, K.Naoi, C.Niwa, Y.Kubota, A.Fujishima, Nat. Mater. 2 (2003) 29.

[21] O.P.Mikheeva and A.I.Sidorov, Tech. Phys. 48 (2003) 602.

[22] H.W.Verleur, A.S.Barker Jr, and C.N. Berglund, Phys. Rev. 172 (1968) 788.

[23] H.Kakiuchida, P. Jin, S. Nakao, M. Tazawa, Jpn. J. Appl. 46 (2007) L113.

[24] J.B.Kana Kana, J.M.Ndjaka, P.Owono Ateba, B.D.Ngom, N.Manyala, O. Nemraoui, A.C. Beye, M.Maaza, Appl. Surf. Sci. 254 (2008) 3959.

[25] G. Xu, C.M. Huang, M. Tazawa, P. Jin, D.M. Chen, and L. Miao, Appl. Phys. Lett. 93 (2008) 061911.

[26] E.Cavanna, J.P.Segaud, and J.Livage, Mater. Res. Bull. 34 (1999)167.

[27] R. Binions, C. Piccirillo, R.G. Palgrave, and I.P. Parkin, Chem. Vap. Deposition 14 (2008) 33.

[28] I. Safi, Surf. Coat. Technol. 127 (2000) 203.

[29] J. Musil, P. Baroch, J. Vlcek, K.H. Nam, J.G. Han, Thin Solid Films, 475 (2005) 208.

[30] J.A.Thornton and A.S.Penfold, Cylindrical Magnetron Sputtering in: Thin films Processes, edited by J.L. Vossen and W. Kern, Academic Press, New-York, 1978, p75.

[31] D.A. Glocker, Proceedings of the Annual SCV Technical Conference (1995), p. 298.

[32] D.E.Siegfried, D.Cook, Ion Tech, Inc., Ft.Collins, CO; D.Glocker, Isoflux,Inc., Rush, NY, 39th Annual Technical Conference Proceedings of the Society of Vacuum Coaters 505/856 (1996) 97.

[33] J. A. Thornton and V. Hedgcoth, J. Vac. Sci. Technol. 12 (1975) 93.

[34] J. T. Cheung, I.M. Gergis, J. James and R. E. DeWames, Appl. Phys. Lett. 60 (1992) 3180.

[35] J. A Greer and H. J. Van Hook, Mater. Res. Soc. Symp. Proc. 191 (1990) 171.

[36] V.W. Lindberg. A.R. Woodard and D.A. Glocker, Surf. Coat. Technol. 133/134 (2000) 484.

[37] A.A. Pradhan, S.I. Shah, K.M. Unruch, Rev. Sci. Instrum. 73 (2002) 3841.

[38] E. Xenogiannopoulou, P. Aloukos, S. Couris, E. Kaminska, A. Piotrowska, E. Dynowska, Opt. Com. 275 (2007) 217.

[39] A.E. Delahoy, S.Y. Guo, C. Paduraru and A. Belkind, J. Vac. Sci. Technol. A 22(4) (2004) 1697.

[40] B.D.Cullity, Elements of X-ray diffraction, 2nd edn, Addison-Wesley, Reading, Mass.1978, p.102.

[41] A.A. Bukharaev, E.F. Kukovitski, D.V. Ovchinnikov, N.A. Sainov, and N.I. Nurgazizov, Phys. Solid State 39 (1997) 1846.

[42] C. Teichert, J.F. Mackay, D.E. Savage, M.G. Lagally, M. Brohl, and P. Wagner, Appl. Phys. Lett. 66 (1995) 2346.

[43] A.A. Fraerman, S.V. Gaponov, B.A. Gribkov, V.L. Mironov, and N.N. Salashchenko, Phys. Low-Dimens. Semicond. Struct. (2002) 79.

[44] V.W. Stone, A.M. Jonas, B. Nysten, and R. Legras, Phys. Rev. B 60 (1999)5883.

[45] V.L. Mironov, O.G. Udalov, B.A. Gribkov, and A.A. Fraerman, J. Appl. Phys. 104 (2008) 064301.

[46] K.L. Kelly, E. Coronado, L.L. Zhao, G.C. Schatz, J. Phys. Chem. B.107 (2003) 668.

[47] M. Futaki and M. Aoki, Jpn. J. Appl. Phys. 8 (1969) 1008.

[48] M.Borek, F.Quian, V.Nagabushnam, and R.K.Singh, Appl. Phys. Lett. 63 (1993) 3288.

[49] F.C.Case, J. Vac. Sci. Technol. A 2 (1984) 1509.

[50] J.F.De Natale, P.J. Hood, and A.B. Harker, J. Appl. Phys. 66 (1989) 5844.

Figure captions

Figure 1: Schematic illustration of the inverted cylindrical magnetron (ICM) sputter gun. The target is the cylindrical ring vanadium metal in which a triangular slice of gold was stuck. The circular magnets were enclosed behind the target. The anode and cathode (target) are perpendicular to each other and the substrates lie perpendicular to the target.

Figure 2: Indexed XRD patterns of Au-VO_2 nanocomposites (background-subtracted; JCPDS 82-661 for VO_2 monoclinic and JCPDS 04-0784 for gold face-centered cubic Fm3m) films sputtered at different substrate temperature ranging from 400 ^{o}C to 600 ^{o}C.

Figure 3: Relationship between the substrate temperature and the particle sizes of Au (square) and VO_2 (dot) estimated from Scherrer's formula.

Figure 4: AFM topographic images of samples sputtered at substrate temperatures (a) 400 ^{o}C; (b) 600 ^{o}C.

Figure 5: X-ray reflectivity profile of Au-VO_2 thin film on Corning glass substrate sputtered at 550 ^{o}C. The circles correspond to the experimental data and solid line the simulation.

Figure 6: Optical transmittance (%) of Au-VO_2 thin films sputtered onto Corning glass at different substrate temperatures for spectra taken at temperature below and above the transition temperature (Tc = 68 ^{o}C) of the host matrix VO_2.

Figure 7: Transmittance at a wavelength of 1100 nm for Au-VO_2 thin films sputtered at 400 ^{o}C and 600 ^{o}C as a function of the external temperature stimuli.

Figure 8: Absorbance spectra of the Au-VO_2 nanocomposite films sputtered at 400 ^{o}C and 600 ^{o}C. Measurements taken below and above the transition temperature Tc = 68 ^{o}C.

Figure 9: Variation of surface plasmon resonance wavelength as function of external temperature stimuli of Au-VO_2 samples sputtered at 400 ^{o}C and 600 ^{o}C.

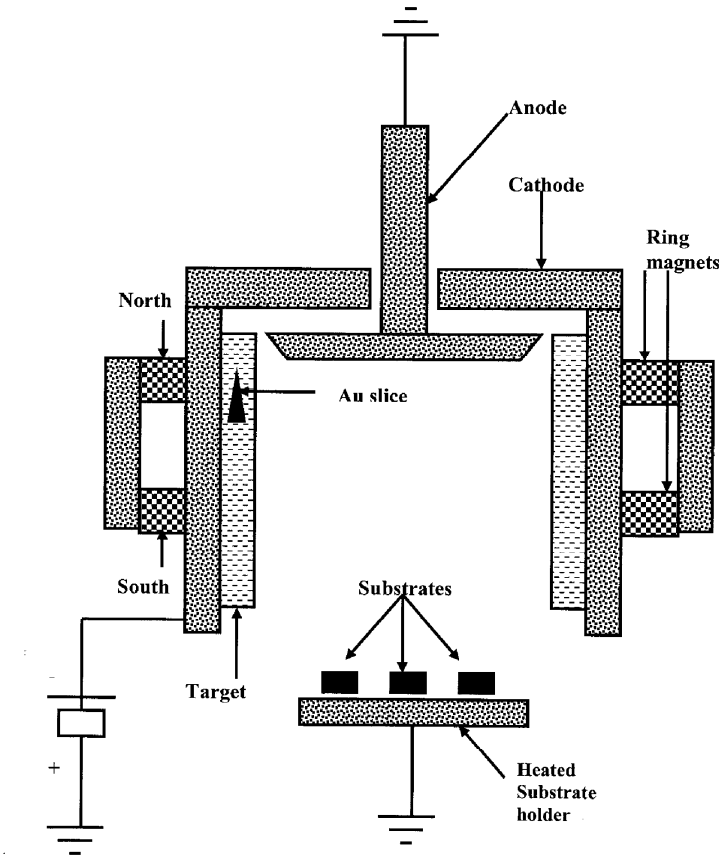

Figure 1: Schematic illustration of the inverted cylindrical magnetron (ICM) sputter gun. The target is the cylindrical ring vanadium metal in which a triangular slice of gold was stuck. The circular magnets were enclosed behind the target. The anode and cathode (target) are perpendicular to each other and the substrates lie perpendicular to the target.

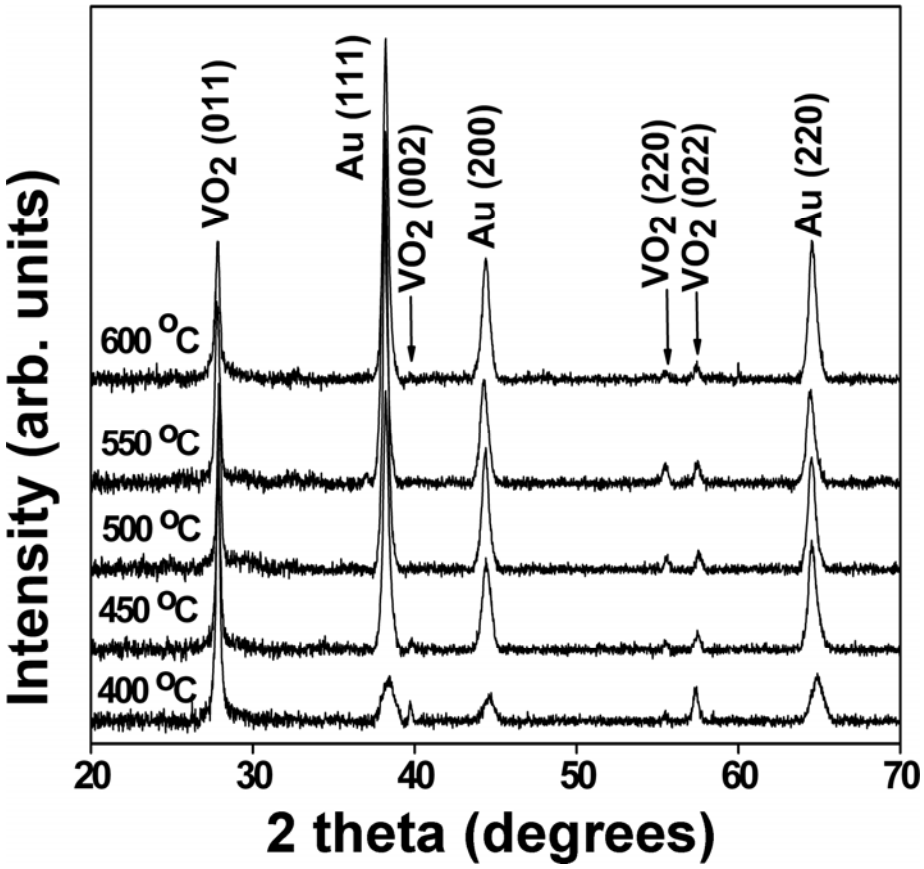

Figure 2: Indexed XRD patterns of Au-VO_2 nanocomposites (background-subtracted; JCPDS 82-661 for VO_2 monoclinic and JCPDS 04-0784 for gold face-centered cubic Fm3m) films sputtered at different substrate temperature ranging from 400 ^{o}C to 600 ^{o}C.

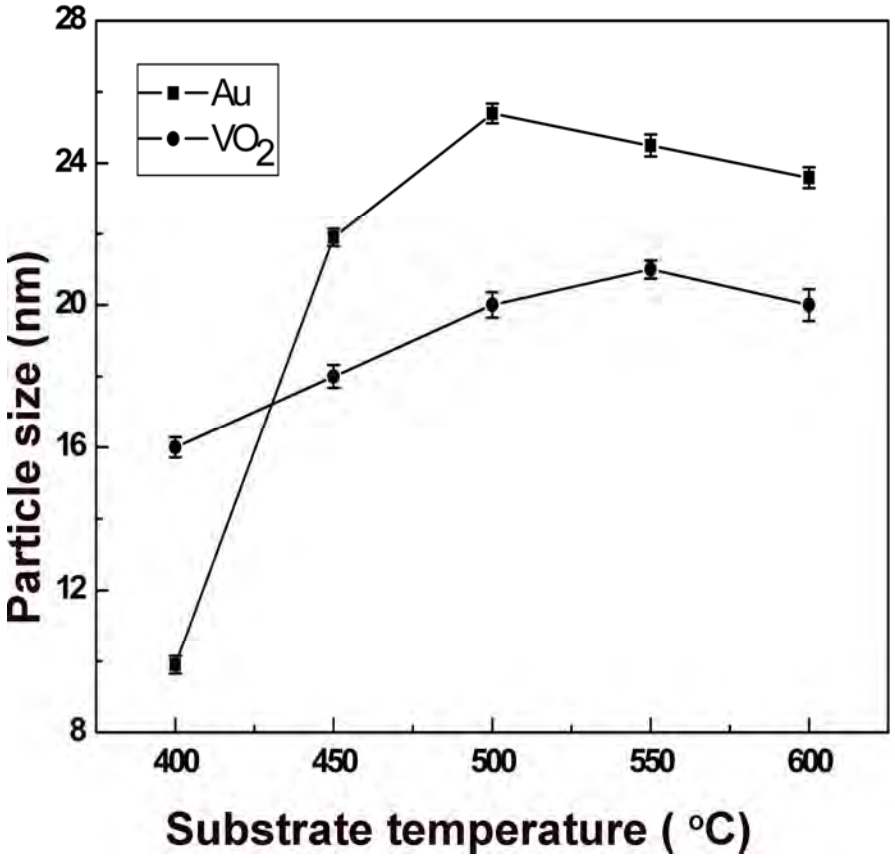

Figure 3: Relationship between the substrate temperature and the particle sizes of Au (square) and VO_2 (dot) estimated from Scherrer's formula.

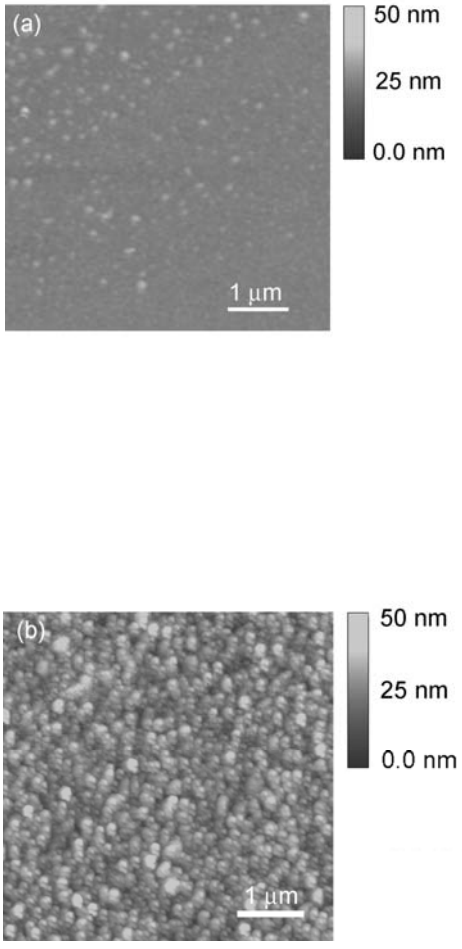

Figure 4: AFM topographic images of samples sputtered at substrate temperatures (a) 400 ^{o}C; (b) 600 ^{o}C.

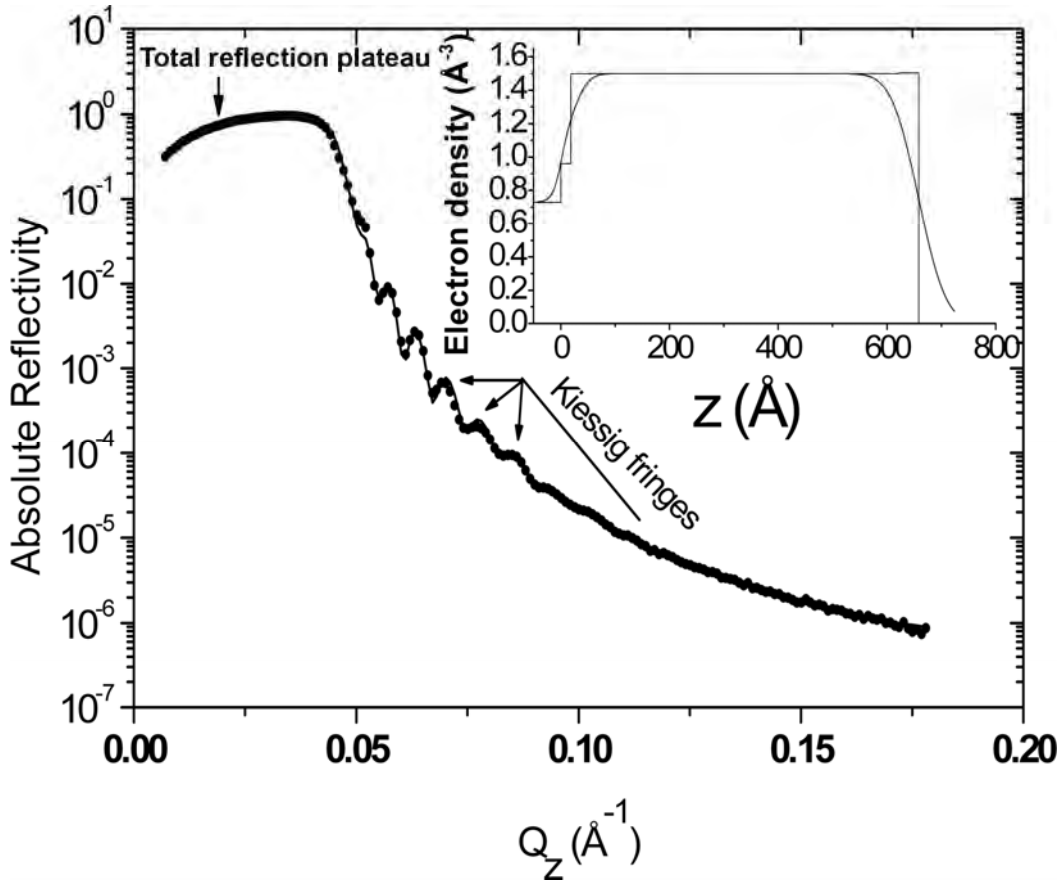

Figure 5: X-ray reflectivity profile of Au-VO_2 thin film on Corning glass substrate sputtered at 550 ^{o}C. The circles correspond to the experimental data and solid line the simulation.

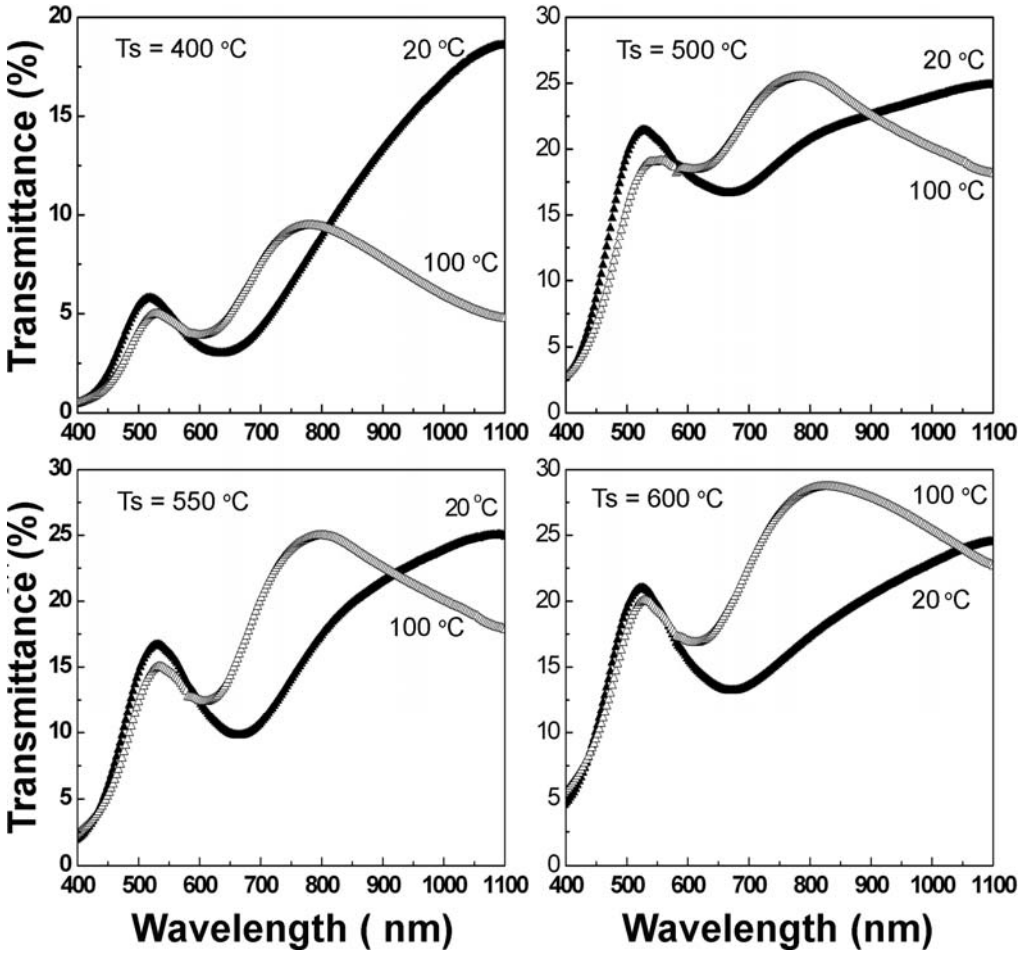

Figure 6: Optical transmittance (%) of Au-VO_2 thin films sputtered onto Corning glass at different substrate temperatures for spectra taken at temperature below and above the transition temperature (Tc = 68 ^{o}C) of the host matrix VO_2.

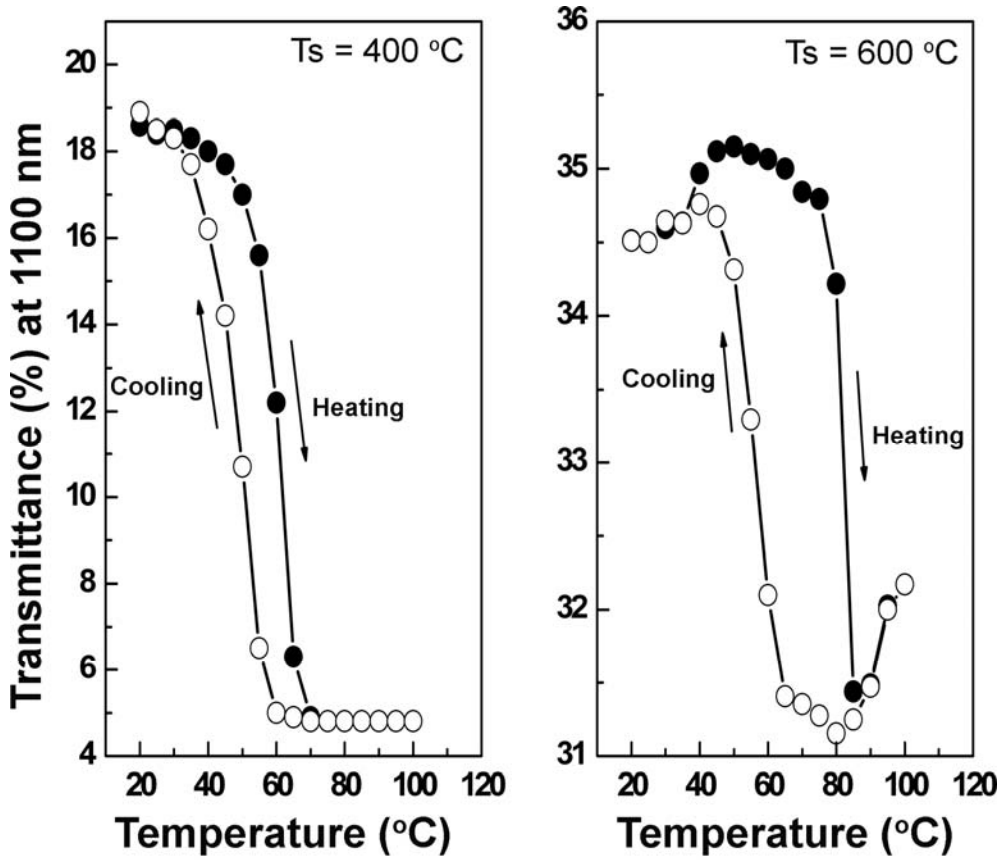

Figure 7: Transmittance at a wavelength of 1100 nm for Au-VO_2 thin films sputtered at 400 ^{o}C and 600 ^{o}C as a function of the external temperature stimuli.

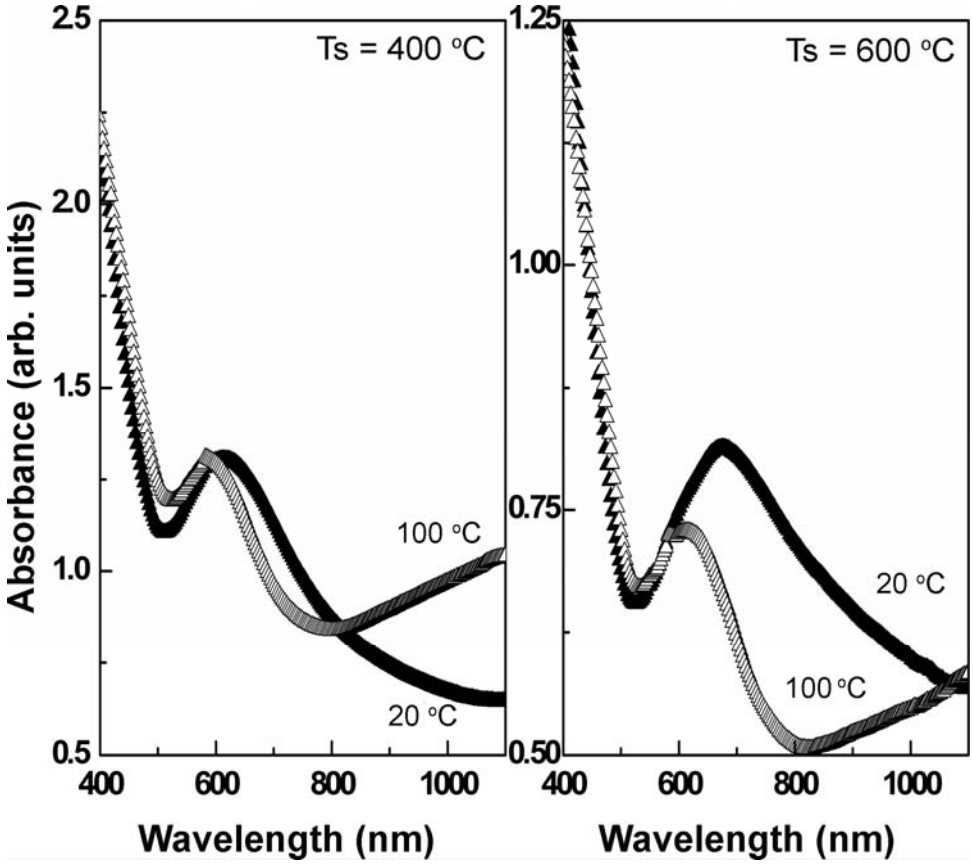

Figure 8: Absorbance spectra of the Au-VO_2 nanocomposite films sputtered at 400 ^{o}C and 600 ^{o}C. Measurements taken below and above the transition temperature Tc = 68 ^{o}C.

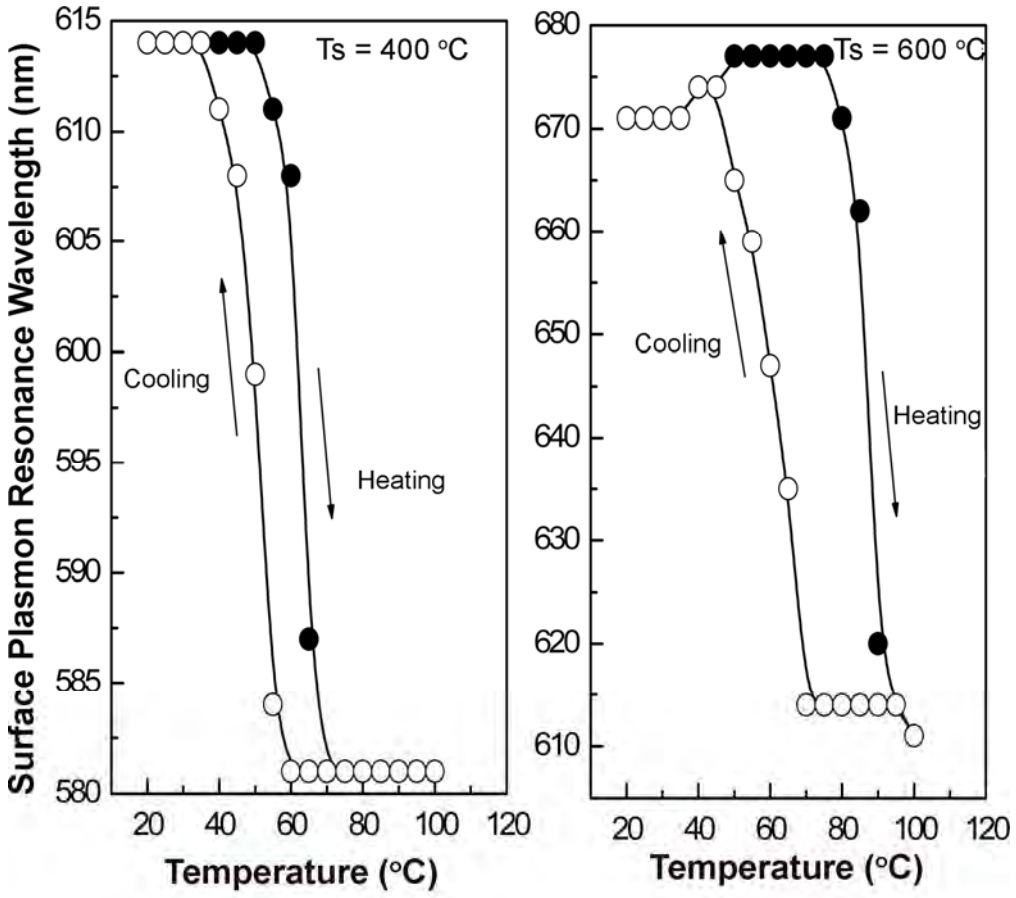

Figure 9: Variation of surface plasmon resonance wavelength as function of external temperature stimuli of Au-VO_2 samples sputtered at 400 ^{o}C and 600 ^{o}C.